

Feasibility of molecular-resolution fluorescence near-field microscopy using multi-photon absorption and field enhancement near a sharp tip

Yoshimasa Kawata,^{a)} Chris Xu, and Winfried Denk^{b)}
Bell Laboratories, Lucent Technologies, Murray Hill, New Jersey 07974

(Received 26 August 1998; accepted for publication 26 October 1998)

Aperture-based near-field microscopy suffers from fundamental limitations imposed by the electromagnetic skin depth of the aperture material and a rapidly decreasing throughput as the aperture is made smaller. Apertureless approaches without these limitations have been demonstrated for coherent imaging but are not easily applicable to incoherent processes such as fluorescence or Raman scattering and to photochemical surface modification. Using multi-photon processes in conjunction with the field enhancement that occurs at a sharp tip in close apposition to a substrate should permit substantial localization of absorption and excitation to a nm sized volume. The expected enhancement of the optical field at the tip edge is calculated here for various combinations of metallic and nonmetallic tip and substrate materials. It is estimated that when using 100 fs pulses repeating at 100 MHz average laser powers of about 10 mW should be sufficient to reach saturating field strengths for three-photon absorption. Steady state and instantaneous temperature rises at the tip are estimated and found likely not to be a limiting factor. Fluorescence quenching is expected to limit the resolution achievable with metallic tips to about 5 nm, but tips made from highly refracting insulators or semiconductors should allow truly molecular resolution. © 1999 American Institute of Physics. [S0021-8979(99)05303-7]

I. INTRODUCTION

Near-field scanning optical microscopy (NSOM) is increasingly applied to a variety of imaging problems.¹⁻⁴ The prevailing probe type for fluorescence imaging still is the melt-pulled tapered optical fiber that is then coated with metal so as to leave a sub-wavelength aperture at the tip.² For tapered fiber probes the achievable resolution is limited fundamentally by the skin depth of the coating material and in practice also by signal-to-noise considerations since the light transmission decreases rapidly as the aperture becomes smaller.⁵ This precludes imaging at truly molecular or atomic resolution and limits the achievable rate of image acquisition thereby making, for example, the observation of fast dynamic phenomena impossible. Furthermore, optical data storage is crucially dependent on high write and readout rates.

To overcome these limitations, several apertureless schemes have been proposed and some of them have been experimentally demonstrated. High resolution imaging has been observed with several coherent methods (detecting elastically scattered light) such as particle plasmon resonance,⁶ or dipole-dipole interactions between tip and sample.^{4,7,8} Coherent schemes are, however, not applicable to most processes with high molecular sensitivity such as Raman scattering or fluorescence. Localization of surface modification using optical field enhancement on tunneling tips has been demonstrated.^{9,10} Light emission during electron tunneling¹¹⁻¹⁶ has been used to define the point of emis-

sion with atomic resolution but there excitation doesn't occur via the optical field and the possibility of excitation spectroscopy is lost.

In this article we consider the practical feasibility of a slightly different approach that also doesn't require an aperture but exploits the substantial local enhancement in the electrical field strength that can occur near and in between sharp geometrical structures,¹⁷⁻²⁰ sometimes called the "lightning rod" effect. Together with nonlinear optical processes such an enhancement is expected to produce true confinement of optical excitation to nanoscopic volumes.^{9,10,19,20} As a particular embodiment of this approach we considered in detail three-photon absorption of light above 1200 nm to excite fluorophores emitting visible light. To study the behavior of the optical near field at molecular dimensions we used as in Ref. 19 (see also Fig. 1) the electrostatic (nonretarded) approximation for a class of geometries which allow the solution to be expressed in terms of Legendre functions of degree ν (see also Eqs. (A1)-(A14) of the Appendix) because we were particularly interested in the scaling behavior at deep sub-wavelength distances, the dependence of enhancement exponents on tip geometry and materials, and the question of "substantial" localization.

II. TRUE LOCALIZATION OF EXCITATION

When actual molecular excitation rather than elastic scattering is to be used in near-field imaging it becomes of central importance that excitation itself is spatially confined rather than merely restricting the volume within which a modulation of the signal occurs as a result of, for example, an oscillating tip-sample distance.^{7,8} The reasons are twofold: (1) background excitation, even when unmodulated,

^{a)}Current address: Shizuoka University, Johoku, Hamamatsu, Japan.

^{b)}Author to whom correspondence should be addressed; electronic mail: denk@bell-labs.com

TABLE I. Enhancement exponents, enhancement factors for three-photon absorption on the substrate ($|E_{\text{sub}}|^6$), and right underneath (see Appendix D) the tip ($|E_{\text{max}}|^6$), required average laser powers [$\langle P \rangle$ (mW)] to reach absorption saturation on the substrate, estimated temperature rise during a single pulse (ΔT_i), and steady state temperature rise (ΔT_s), assuming 100 fs pulses at 100 MHz repetition rate at 1500 nm wavelength, 10 nm tip radius, and a tip opening angle of 45° .

Tip/gap/ subs.	ν	$ E_{\text{max}} ^6$	$ E_{\text{sub}} ^6$	$\langle P \rangle$ (mW)	ΔT_i ($^\circ$)	ΔT_s ($^\circ$)
Au/air/Au	-0.0415	4.1×10^8	5.8×10^6	3.2	26	0.0055
Au/air/diamond	0.132	1.5×10^7	1.5×10^5	11	30	0.0092
Ir/Air/diamond	0.127-0.0257I	1.6×10^7	1.6×10^5	11	3.4×10^2	0.3
W/Air/diamond	0.112-0.1I	7.2×10^7	5.7×10^5	6.8	1.9×10^3	0.96
Pt/air/diamond	0.144-0.037I	1.2×10^7	1.2×10^5	11	5.2×10^2	0.97
Si/airdiamond	0.342	2.8×10^5	5.1×10^3	33	2.9	0.0007
Si/air/silicon	0.292	7.2×10^5	1.6×10^4	23	2.6	0.0005
diamond/air/diamond	0.49	1.7×10^4	5.3×10^2	70

leads to photodamage or photoconversion in molecules outside the focal area or volume; (2) in the case of fluorescence excitation, fluorescence light stemming from molecules outside the modulation volume doesn't create additional signal, but still generates photon shot noise, which can easily overwhelm the signal from molecules of interest inside the focal volume. As the focal volume we consider the volume around the probe tip where the field strength is of the same order as the peak field strength. The size of this volume determines the achievable resolution.

Excitation localization to volumes about 10 nm across is easily achieved using small apertures^{1,21} but is difficult without an aperture, if linear absorption is considered and no use is made of a resonance condition such as a particle plasmon.^{6,22} The use of a resonance, while offering substantial enhancements and true localization, severely restricts the choice of wavelengths and materials. For particle resonances, the reduction of Q with decreasing particle size furthermore limits the attainable resolution.²³

Substantial excitation localization without an aperture or resonance can, on the other hand, be easily achieved with nonlinear optical processes, as we will argue. Due to their much stronger dependence on the field strength, higher order (≥ 2) nonlinear processes require a much smaller enhancement of the electrical field than linear processes to get a certain enhancement of the excitation rate. For a process where multiple (n) photons are absorbed simultaneously the rate depends on the ($2n$)th power of the local electrical field and even moderate enhancements in the field strength lead to substantial localization of excitation. The criterion of substantial localization that we use is that a sizable fraction of all molecular excitations should occur in a small volume. This can be illustrated using an example from far-field optics: linear (single-photon) absorption versus multi-photon absorption in a focused laser beam.^{24,25} In the one-photon case, even though the molecular excitation rate falls rapidly away as the distance (r) to the focus increases, the total amount of excitation within, say, a volume bound by the half-intensity surface of the beam, is only an infinitesimal

fraction of the light generated in an infinite sample since each additional volume shell of a given thickness contributes a roughly equal amount of excitation. This is the very reason that optical sectioning requires the use of a confocal pinhole when one-photon excitation is used. For multi-photon excitation, on the other hand, most of the excitations occur within a small volume and each additional volume shell contributes an amount that decreases with $r^{-(2n-2)}$, leading to a rapid convergence of the total fluorescence.²⁶ Optical sectioning can therefore be achieved during excitation alone. This yields an almost complete elimination of photochemical side effects, such as photobleaching, outside the immediate focal volume.

By applying the same reasoning to tip enhancement, i.e., near-field microscopy, we find that the absorption probability has to fall off faster than r^{-3} to lead to true confinement in three dimensions (r^{-2} for a two-dimensional distribution of absorbers, e.g., on the substrate surface). Following the treatment of Ref. 19, it becomes clear that even for the lowest possible fractional degree $\nu = -0.5$ [the asymptotic behavior of the field away from the tip is proportional to $r^{\nu-1}$ and that of n -photon absorption to $(r^{\nu-1})^{2n}$] the r^{-3} condition is only marginally reached for one-photon absorption and the number of excitations still diverges logarithmically.¹⁹ An additional restriction is that in order to achieve that tip resonance ($\nu = -0.5$) one would have to use a particular wavelength, at which even for the best tip materials such as gold and silver there still is significant absorption not to mention the limitation to molecules absorbing at such wavelengths. N -photon absorption, on the other hand, provides true confinement without such stringent conditions. Instead we only need to fulfill $\nu < \nu_{3d} = 1 - 3/2n$ and $\nu < \nu_{2d} = 1 - 2/2n$ for three- and two-dimensional absorber distributions, respectively. The general relation is $\nu < 1 - d/2n$, where d is the dimension of the chromophore distribution and n is the order of the absorption process. For $n = 3$ this condition can be met both for two- and three-dimensional fluorophore distributions using a wide range of materials over a wide range of wavelengths (Table I, Figs. 2-4). It is worth noting that even

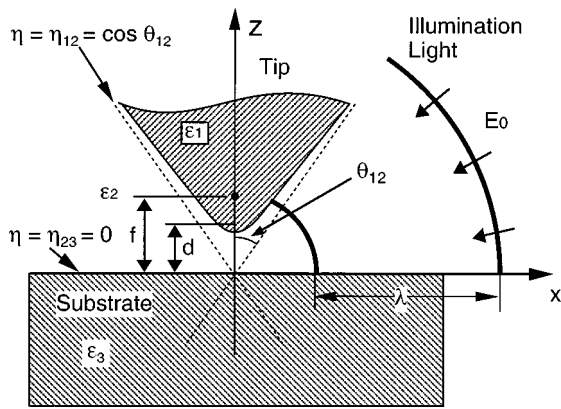


FIG. 1. Tip/sample geometry used in our calculations. In prolate spherical coordinates tip and substrate surfaces both are surfaces of constant η ($\eta = \cos \theta_{12}$ and $\eta = \cos \theta_{23} = \cos(\pi/2) = 0$, respectively). This allows a separation of variable for the partial differential equations for the field (see Refs. 19 and 42).

for dielectric tips the field strength diverges in the case of vanishing tip radius. This is very different from the case of an ellipsoid where for dielectric materials the field enhancement is limited to ϵ -fold even in the case of an arbitrarily pointed prolate shape.²³

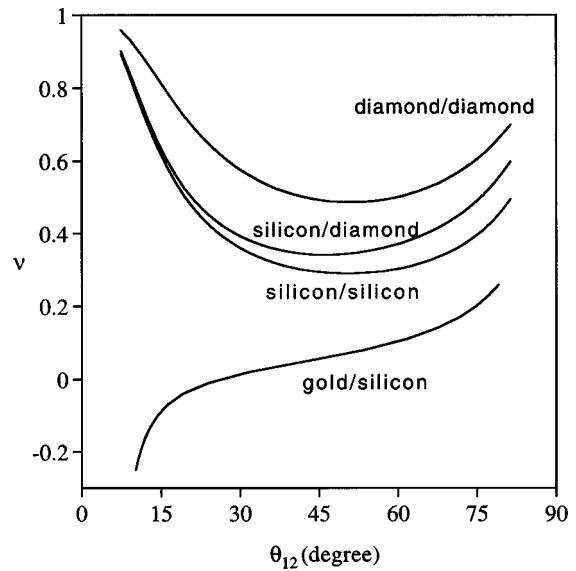


FIG. 3. Field enhancement exponent ν as a function of tip opening angle for different combinations of tip/substrate materials.

A closer look at the enhancement exponent as a function of various parameters reveals a number of interesting features. As expected, there is field enhancement even in the absence ($n_3 = 1$) of the substrate, which in the case of the ideal metal ($\epsilon_1 = -\infty$) would be sufficient for substantial localization of three-photon excitation in three dimensions for tips with 45° half opening angle [Fig. 2(a)]. Even steeper enhancement is expected for tips made of real metals such as gold [Fig. 2(b)]. A conspicuous difference between metals ($n_1 < 0$ and dielectrics $n_1 > 1$) is the behavior towards more acute tip opening angles (Fig. 3), where metals tend to have their biggest enhancement while dielectrics peak at around 45° . A comprehensive overview for the behavior of dielectrics is given in Fig. 4 for three different opening angles (10° , 45° , and 80°). As expected from Fig. 3, the biggest enhancement is seen at approximately 45° . The contours at $\nu = 5/6$, $2/3$, and $1/2$ indicate the boundaries of true confinement for one-, two-, and three-dimensional absorber distribution, respectively.

We calculated the point-spread functions (see also Appendix B) for gold tips [Fig. 5(a)] and silicon tips [Fig. 5(b)], both over diamond substrates. For silicon, which provides comfortable confinement at 45° , ν is at the edge of the confinement boundary at 80° and outside for 10° , and the point-spread function depends strongly on the tip opening angle. Less dependence on the tip angle is found for gold, where we are well within the confinement boundaries for all angles.

To get a sense for the degree of confinement, we estimated the fraction of the total excitation actually localized to the focal volume, here defined as bounded by the surface of half maximal excitation (see Appendix E). Figure 6 shows the results as a function of ν for two-dimensional absorber distributions and for $n = 1, 2$, and 3 . The fraction, of course, becomes 0 as soon as ν crosses the confinement boundary. It is worth noting that the confinement ratio increases steeply below the limit so that even with ν close to the confinement boundary microscopy should be possible.

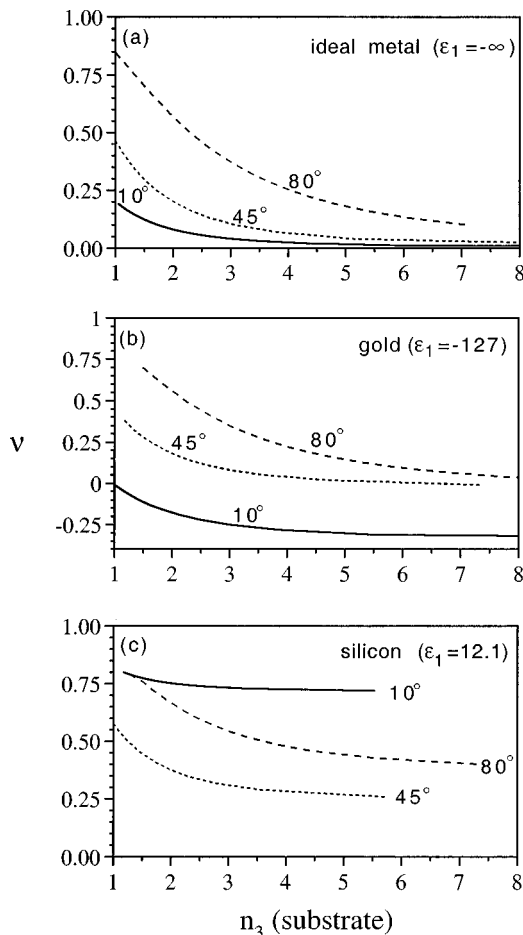


FIG. 2. Field enhancement exponent ν for different tip materials and opening angles θ as a function of the substrate refractive index n_3 . (a) Ideal metal, (b) gold, (c) silicon.

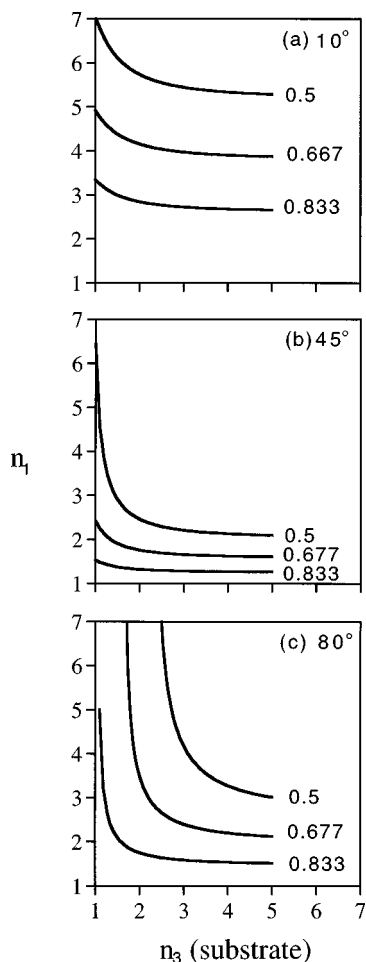


FIG. 4. Contour plots of ν as it varies as a function of tip and substrate refractive indices for three different tip opening angles. (a) 10° , (b) 45° , and (c) 80° . The limits of convergence ($\nu=5/6$, $2/3$, $1/2$) for one-, two-, and three-dimensional absorber distributions and three-photon absorption are indicated by thicker contour lines.

As we can see, sufficient enhancement for true confinement should exist in the three-photon case even for tips made out of diamond, silicon, or silicon carbide (Table I). Micro-fabricated silicon tips, with a radius of curvature of less than 10 nm, integrated into force microscopy levers, are readily available commercially (Digital Instruments, Park Scientific). Because silicon is not absorbing above about 1200 nm, large excitation intensities can be used without heating the tip by one-photon absorption. A practical advantage of multiphoton excitation is the easy discriminability of the fluorescence light from the excitation light due to the large wavelength difference between excitation and emission wavelength.

III. LASER POWERS AND PULSE WIDTHS

To evaluate the feasibility of using tip-enhanced multiphoton excitation at high scan rates we calculated the average laser power necessary to saturate the fluorescence excitation of a molecule on the substrate right beneath the apex of the tip (see also Appendix C). Saturation, beyond which an increase in intensity doesn't increase the rate at which fluorescent photons are created, means that about one ab-

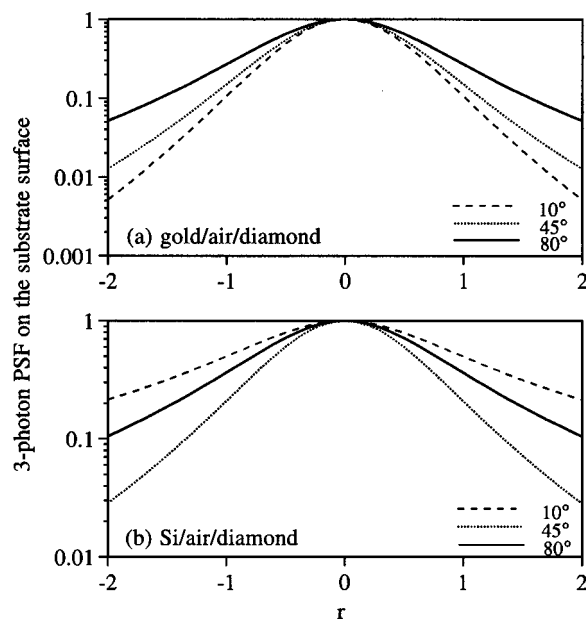


FIG. 5. The expected point-spread function along the substrate surface for different tip opening angles calculated for gold tip over diamond surface and for silicon tip over diamond surface (three-photon excitation). The position is expressed in units of the coordinate focal length f .

sorption event occurs per pulse repetition period or per fluorescence decay time, whichever is longer. For the ultrashort pulse lasers that are most common now the repetition period (≈ 10 ns) is longer than the fluorescence decay times for most organic fluorophores,²⁷ in particular when taking the shortening of the excited state lifetime into account that will result from tip and surface effects (see below). To generate about one absorption event per pulse of 100 fs duration in each fluorophore the absorption rate has to be 10^{13} s^{-1} . Together with the typical three-photon absorption cross section²⁸ of $\sigma_3 \approx 10^{-94} \text{ m}^6 \text{ s}^2 (\text{photon})^{-2}$ this yields an esti-

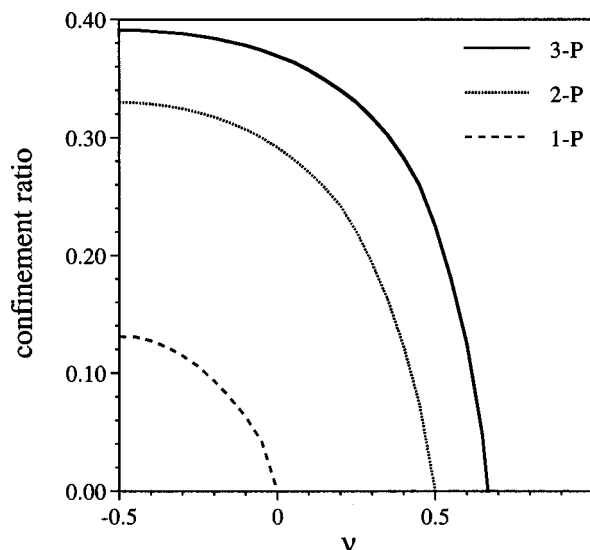


FIG. 6. Ratio of total excitation to the excitation that occurs within a volume bounded by the surface of half maximal excitation as a function of ν for one-, two-, and three-photon absorption for a two-dimensional distributions of absorbers.

mate of the local intensity of about 6×10^{16} W/m², or a field strength of $E_s \approx 4.8 \times 10^9$ V/m. Without any field enhancement but with diffraction limited focusing using a lens with a numerical aperture of about 1, an average power level of several hundred mW is needed to saturate the fluorescence transition.²⁸ After taking the field enhancement due to tips with 10 nm radius of curvature into account the range of average incident powers lies between 3 and 70 mW. We estimated the field enhancement by using the enhancement exponents ν as calculated above.¹⁹ We also assumed that the incident light was focused to a spot roughly 1 μ m across. The results for a variety of material combinations are listed in Table I. The pulse energies required are between 3×10^{-11} and 7×10^{-10} J for three-photon absorption probabilities of order one/pulse. Even the power levels required for dielectric tips are easily achievable with optical parametric oscillators, Cr⁴⁺ lasers²⁹ operating around 1500 nm, or erbium doped fiber lasers.³⁰

The calculated enhancement factors should be reasonably accurate for dielectrics. Inside metallic materials the wavelengths become complex, however, and much smaller, reducing the length scale up to which the electrostatic approximation can be used.³¹

Tip heating

Since heating of the coating material limits the excitation in aperture based near-field microscopy to rates many orders of magnitude below the saturation regime, we estimated the heating of the tip for the apertureless configuration to insure that saturating excitation can, in fact, be used. We assumed saturating pulse energy levels and linear, i.e., one-photon, absorption using bulk optical constants for metallic tips. Two separate time scales have to be considered. First, there is the instantaneous temperature rise that occurs during a single pulse at the point of maximal field enhancement. For a pulse duration of 100 fs thermal conduction is negligible even for the dimensions of the order of the tip radius (for a distance of 10 nm the thermal diffusion time is around 1 ps for gold). The volume density of energy (q) dissipated during a single pulse is given by

$$q = \omega \epsilon_i E_i^2 \tau_p, \quad (1)$$

where ω is an angular frequency of light, $\epsilon_i = \text{Im}(\epsilon)$, τ_p is the pulse length, and E_i is the electric field just inside the tip surface, its value related to the field outside the tip E_{out} by $E_i = E_{\text{out}} \epsilon_2 / \epsilon_1$ for the perpendicular component. For symmetry reasons the parallel component of the electric field is zero at the apex and it can be easily shown that the point of maximum field strength occurs at the apex both inside and outside the material. The instantaneous temperature rise ΔT_i caused by a single pulse at the point of maximum field enhancement is thus

$$\Delta T_i = \tau_p \omega \epsilon_i [E_{\text{max}} \epsilon_2 / \epsilon_1]^2 / c_p, \quad (2)$$

where c_p is the heat capacity of the tip material. Predictably, the largest temperature rises occur for strongly absorbing metals like Pt, Ir, and W, which otherwise would be suitable tip materials due to their mechanical properties and their known ability to form and maintain sharp tips. The best

metal—from an optical but not mechanical viewpoint—is gold, with about 30° of temperature rise. These values for ΔT_i are likely to still be overestimates because, as in vacuum tunneling of electrons, the energy is initially present in the form of hot electrons and is transferred to the lattice throughout a larger volume, determined by the mean free path.

Next we estimated the steady state temperature rise. To simplify the problem we approximated the hyperboloid tip as a cone, which is illuminated up to a distance of $\lambda / (2\pi)$ from the tip. Such an approximation overestimates the temperature rise by enlarging the volume where heat is produced. This is especially the case for metallic tips because the skin depths of good conductors are only on the order of nanometers. The maximum temperature rise occurs at the tip of the cone and can be calculated as³²

$$\Delta T_{\text{max}} = \int_0^{\lambda/(2\pi)} \frac{\omega \epsilon_i |E|^2}{\kappa r} r^2 dr, \quad (3)$$

where κ is the thermal conductivity. To obtain an analytically tractable expression of Eq. (3), we further approximate the E field as

$$E = \begin{cases} E_{\text{max}} \frac{\epsilon_2}{\epsilon_1}, & \text{for } r \leq r_0 \\ E_{\text{max}} \frac{\epsilon_2}{\epsilon_1} \left(\frac{r_0}{r}\right)^{1-\nu}, & \text{for } r > r_0 \end{cases}, \quad (4)$$

where r_0 is the radius of curvature of the tip. Here we have utilized the asymptotic behavior of the E field.¹⁹ The maximum temperature rise is then given by

$$\Delta T_{\text{max}} = \frac{\omega \epsilon_i |\epsilon_2 / \epsilon_1 E_{\text{max}}|^2 r_0^2}{2\kappa} \times \left[1 - \frac{1}{\text{Re}[\nu]} + \frac{1}{\text{Re}[\nu]} \left(\frac{\lambda}{2\pi r_0}\right)^{2 \text{Re}[\nu]} \right], \quad (5)$$

where $\text{Re}[\nu]$ denotes the real part of ν . Examples of the calculated values are listed in Table I.

Heating by linear absorption should be negligible for transparent dielectrics such as silicon. However, strongly doped silicon does show significant free carrier absorption at 1500 nm, which may rule out the use of tips that are fabricated using the dissolved wafer process which requires very high dopant levels. Heating caused by two-photon excitation in silicon can also be estimated using the above models except that two-photon absorption cross section has to be used and the heat deposition is now proportional to $|E|^4$. For the values listed in Table I, we have used a two-photon absorption coefficient of ~ 1.0 cm/GW for silicon (Xu and Denk, unpublished result). Clearly two-photon heating is negligible even at the intensity necessary for three-photon saturation on the substrate.

IV. PITFALLS

A. Quenching of fluorescence

Fluorescence emission from a molecule can be severely affected by the proximity of a surface.^{33,34} Metallic surfaces, in particular, pose a problem for tip-enhanced excitation of

fluorescent molecules, since these molecules can lose their energy via radiationless energy transfer to the tip or the substrate material if either of those is strongly absorbing at the emission wavelength. Quenching by an absorbing substrate material is stronger than by an absorbing tip because the molecules to be imaged tend to be located at the substrate surface rather than on the tip. The use of an absorbing substrate is a disadvantage also because it prohibits, for example, the illumination and detection through the substrate. Following Chance *et al.*^{35,36} we used the following relation to calculate for the extent of quenching:

$$b_{\text{ET}} = \left(\frac{q}{k_f^3 d^3} \right) \left(\frac{3 \epsilon_2 n_1 \kappa_1}{2 |\epsilon_1 + \epsilon_2|^2} \right), \quad (6)$$

where k_f , n_1 , and κ_1 are the wave number of the fluorescence, the refractive index, and the extinction coefficient of tip material, respectively, and q is the quantum yield of the emitting state in vacuum.

The loss of fluorescence light due to quenching is somewhat reduced by the increased emission rate due to the field enhancement effect. Emission, however, is a first order process and its enhancement, with a much weaker dependence on the characteristic length, cannot fully compensate quenching, which increases like d^3 for small distances. This limits the resolution that is achievable for fluorescence excitation with metallic tips to about 5 nm. The use of Si tips improves the situation somewhat but still requires a distance between tip and fluorophore of at least 2 nm.

To increase the spatial resolution to atomic dimensions, a dielectric tip material that is nonabsorbing at the emission wavelength has to be used. Even those dielectric materials with the largest known refractive indices provide smaller enhancement exponents (ν) than metals or semiconductors (Table I). The exponents are, however, still large enough to provide true confinement [$\nu < 1 - d/(2n)$] for \geq three-photon excitation. For example, if we use diamond on a diamond surface ν is about 0.49, well within the region of true confinement [Fig. 4(b)] for a two-dimensional absorber distribution. For intermediate resolution metallic tips may be preferable because they generate larger field enhancements even at moderate wavelength-to-tip radius ratios. For the ultimate resolution in fluorescence microscopy transparent tips are, however, necessary to avoid emission quenching.

B. Nonlocality of refractive index

Our calculations so far were based on the assumption that the refractive index is local, i.e., the polarization depends only on the local electrical field. This assumption becomes invalid for length scales below the mean free path of charge carrier in metals, as is, for example, manifest in surface effects which reduce the effective conductivity in small particles.²³ Nonlocal refractive index effects are likely to reduce the actual enhancement in the case of very sharp metal tips but not for dielectrics, which don't have mobile electrons. Like fluorescence quenching, nonlocality effects ultimately favor dielectric tips and substrate material over metals at molecular dimensions.

C. Dielectric breakdown

The intensities required for dielectric breakdown vary strongly with the pulse width and no direct measurements are available for the 1500 nm wavelength regime. Measurements at shorter wavelength, where the damage fluence for fused silica was measured,³⁷ yielded a value of about 2×10^4 J/m² for 500 fs pulses at 1053 nm for both fused silica and CaF₂. The extrapolation of the theory used to interpret these results and some data for 150 fs pulses at 825 nm suggest a peak power damage threshold of about 10^{17} W/m². This value is comparable to the local intensities required for three-photon saturation ($\sim 6 \times 10^{16}$ W/m²). Although the intensities inside the tip and the substrate are reduced by factors of ϵ_1^2 and ϵ_3^2 , respectively, surface breakdown may occur at such high intensities, especially taking into account that the intensity right underneath the tip is higher than that on the substrate (Table I). Dielectric breakdown could therefore limit the achievable three-photon excitation rate to values below singlet saturation.

D. Reduction of the field enhancement by an absorbing molecule

The presence of an absorbing molecule underneath the tip is bound to reduce the local field in analogy to the case of a radio antenna, where the output voltage depends on the load impedance. If the load is comparable or larger than the characteristic output impedance of the antenna the actual field will be considerable smaller than the unloaded field. This, of course, implies that the actual enhancement would also be considerably reduced from its theoretical unloaded value. A crude estimate of this effect can be made by replacing the atom with a small sphere consisting of a lossy dielectric. Given an absorption cross section of $\sigma \approx 10^{-21}$ m² the size of an equivalent sphere with $\text{Im}(\epsilon)$ of order 1 can then be estimated by dimensional analysis as

$$d \approx \sqrt[3]{\sigma \lambda} \approx \sqrt[3]{10^{-21} \text{ m}^2 10^{-6} \text{ m}} \approx 1 \text{ nm}.$$

This implies that a strong distortion of the unloaded field begins at tip radii below 1 nm for linear excitation. The case of nonlinear absorption is complicated by the fact that σ is not a simple property of the molecule but depends on the intensity of the impinging light. At a given intensity I we can, however, define an effective cross-section σ_{eff} . For three-photon absorption

$$\sigma_{\text{eff}} = \delta_3 I^2,$$

where δ_3 is the three-photon absorption cross section. For the case of the saturating intensity, we find $\sigma_{\text{eff}} = \tau^{-2/3} \delta_3^{1/3} \approx 2 \times 10^{-23}$ m² (where τ is the pulse length). This translates into $d_{\text{eff}} \approx 0.3$ nm, comparable to atomic dimensions and therefore not necessarily negligible. But reducing the excitation intensity also reduces σ_{eff} and an arbitrarily small d_{eff} can, therefore, always be achieved, albeit at the expense of the excitation rate.

V. POTENTIAL APPLICATIONS

A. Fluorescence microscopy

Among light microscopy techniques fluorescence microscopy has a special position because of its ability to distinguish between different molecular species with extremely high specificity. For example, it is possible to detect single fluorophore, e.g., labeled biomolecules like proteins and DNA, in a focal volume that contains about 10^8 other molecules.^{38,39} This makes the availability of a fast-scanning molecular-resolution fluorescence near-field technique desirable. Tip-enhanced nonlinear absorption is limited in its resolution only by the tip radius and does not suffer from a reduction of the excitation rate as the resolution is increased. The achievable scan rate is more likely to be limited by the speed of the distance control methods since, even at 1% singlet saturation, a single molecule will emit about 10^6 photons/s, with an overall detection efficiency of, say, 10% a pixel dwell time of 100 μ s, which would give easily detectable ten-photon signals.

B. Localized photochemical modification

Multi-photon excitation provides the necessary localization and, at the same time, allows one to reach the relatively high quantum energies (typically in the UV range for one-photon excitation) that are necessary for the modification of chemical bonds while the incident light is in the red or near infrared. This has been demonstrated of the case of two-photon absorption induced photochemical release of biological agonists⁴⁰ using far-field focusing. In near-field applications an important additional advantage is that, in general, the optical properties (like absorption) of materials that one might use for the fabrication of tips are more favorably in the near infrared wavelength region than in the UV.

C. Optical storage

The use of near-field optics in optical storage has been proposed and demonstrated in principle several years ago⁴¹ using the coated tapered fiber approach. As in the case of microscopy applications, this approach suffers from optical throughput problems that become exacerbated at high resolution, i.e., high storage density. The tip-enhanced nonlinear absorption approach remedies that problem as no reduction of the excitation rate occurs at high resolution and the achievable storage density is not limited by the electromagnetic penetration depth into the coating material.

VI. CONCLUSION

We have evaluated the feasibility of multi-photon excitation using tip-enhancement near-field microscopy. We found that for three or more photon excitation truly localized excitation should be possible with a wide range of tip materials (metals and dielectrics) and geometries. For fluorescence imaging at molecular resolution dielectric tips will be necessary in order to avoid the quenching of the fluorescence emission. The necessary laser powers and pulse width are in

a range that is easily achievable with present technology. Tip or sample destruction by heating is not expected even at saturating three-photon excitation rates.

APPENDIX A: POTENTIAL AND ELECTRIC FIELD IN HYPER PROLATE COORDINATE

Following Ref. 19, the electric potential $V(\xi, \eta)$ can be written as

$$V(\xi, \eta) = \Xi(\xi) \times H(\eta), \quad \xi \geq 1, -1 \leq \eta \leq 1 \quad (\text{A1})$$

in prolate spherical coordinates (ξ, η, φ) , which are converted to Cartesian coordinates (x, y, z) by

$$x = \sqrt{(\xi^2 - 1) \cdot (1 - \eta^2)} \cos \varphi, \quad (\text{A2})$$

$$y = \sqrt{(\xi^2 - 1) \cdot (1 - \eta^2)} \sin \varphi, \quad (\text{A3})$$

$$z = \xi \cdot \eta,$$

where we assumed the distance between the two focal points to be 1.

By considering the electromagnetic boundary conditions at tip and substrate surfaces, we get the following solution for the potential:

$$H(\eta) = \begin{cases} P_\nu(\eta), & \eta \geq \eta_{12} \\ aP_\nu(\eta) + bP_\gamma(-\eta), & \eta_{12} \geq \eta \geq 0, \\ cP_\nu(-\eta), & \eta \leq 0 \end{cases} \quad (\text{A4})$$

$$a = \frac{1 - \epsilon_3}{2} c, \quad (\text{A5})$$

$$b = \frac{1 + \epsilon_3}{2} c, \quad (\text{A6})$$

$$c = \frac{2P_\nu(\eta_{12})}{(1 - \epsilon_3)P_\nu(\eta_{12}) + (1 + \epsilon_3)P_\nu(-\eta_{12})} \quad (\text{A7})$$

and components of the electric field are given by

$$E_x = \frac{\partial V}{\partial x} = \frac{x}{\xi^2 - \eta^2} \left(\xi \frac{\partial V(\xi, \eta)}{\partial \xi} - \eta \frac{\partial V(\xi, \eta)}{\partial \eta} \right), \quad (\text{A8})$$

$$E_y = \frac{\partial V}{\partial y} = \frac{y}{\xi^2 - \eta^2} \left(\xi \frac{\partial V(\xi, \eta)}{\partial \xi} - \eta \frac{\partial V(\xi, \eta)}{\partial \eta} \right), \quad (\text{A9})$$

$$E_z = \frac{\partial V}{\partial z} = \frac{1}{\xi^2 - \eta^2} \times \left[\eta(\xi^2 - 1) \frac{\partial V(\xi, \eta)}{\partial \xi} - \xi(\eta^2 - 1) \frac{\partial V(\xi, \eta)}{\partial \eta} \right]. \quad (\text{A10})$$

Immediately above the substrate surface

$$\begin{cases} \eta = 0, \\ \xi^2 = x^2 + y^2 + 1, \end{cases} \quad (\text{A11})$$

the electric field components are

$$E_x = \frac{x}{\xi} \frac{\partial V(\xi, \eta)}{\partial \xi}, \quad (\text{A12})$$

$$E_y = \frac{y}{\xi} \frac{\partial V(\xi, \eta)}{\partial \xi}, \quad (A13)$$

$$E_z = \frac{1}{\xi} \frac{\partial V(\xi, \eta)}{\partial \eta}. \quad (A14)$$

APPENDIX B: TWO-DIMENSIONAL POINT-SPREAD FUNCTION $p_n(x, y)$ FOR n -PHOTON EXCITATION

Using Eqs. (A11) through (A14), the point spread function $[p_n(x, y)]$ on the substrate surface can be calculated

$$\begin{aligned} p_n(x, y) &= \left| \frac{E(x, y, 0)}{E(0, 0, 0)} \right|^{2n} \\ &= \left| \frac{1}{\epsilon_3 P'_\nu(0)} \right|^{2n} \left| \frac{\xi^2 - 1}{\xi^2} P'^2_\nu(\xi) P^2_\nu(0) \right. \\ &\quad \left. + \frac{\epsilon_3^2}{\xi^2} P^2_\nu(\xi) P'^2_\nu(0) \right|^n. \end{aligned} \quad (B1)$$

APPENDIX C: ELECTRIC FIELD FOR SATURATION

To get about one absorption event per pulse and fluorophore the excitation rate during the pulse needs to be

$$\sigma I^3 \approx \tau_p^{-1}. \quad (C1)$$

For a pulse width of 100 fs and a typical $\sigma_3 \approx 1 \times 10^{-94} [\text{m}^6 \text{s}^2 (\text{photon})^{-2}]$ at a wavelength of 1500 nm, the required peak intensity for saturation is

$$\begin{aligned} I &\approx 4.6 \times 10^{35} [(\text{photon})\text{m}^{-2} \text{s}^{-1}] \times 1.32 \times 10^{-19} [\text{J}(\text{photon})^{-1}] \\ &= 6.13 \times 10^{16} [\text{Wm}^{-2}]. \end{aligned} \quad (C2)$$

Using that $|E_s|^2 = I / (\epsilon_0 C)$ we find

$$|E_s| \approx 4.8 \times 10^9 [\text{V/m}]. \quad (C3)$$

APPENDIX D: CALCULATION OF $|E_{\text{sub}}|^2$ AND $|E_{\text{max}}|^2$

$$|E_{\text{max}}(\xi, \eta)|^2 = |E(1, 0)|^2 = |c \epsilon_3 P'_\nu(0)|^2, \quad (D1)$$

$$\begin{aligned} |E_{\text{sub}}(\xi, \eta)|^2 &= |E(1, \eta_{12})|^2 \\ &= \left| \frac{c}{2} [(1 - \epsilon_3) P'_\nu(\eta_{12}) - (1 + \epsilon_3) P'_\nu(-\eta_{12})] \right|^2. \end{aligned} \quad (D2)$$

APPENDIX E: FRACTION OF TOTAL EXCITATION THAT OCCURS WITHIN THE HALF MAXIMUM EXCITATION

By integrating the point-spread function we can calculate the fraction of the signal that is generated in the ‘‘focal’’ region

$$R_n = \frac{\iint_{D_{1/2}} p_n(x, y) dx dy}{\iint_{\text{space}} p_n(x, y) dx dy} = \frac{\int_1^{\xi_n} p_n(\xi) \cdot \xi d\xi}{\int_1^\infty p_n(\xi) \cdot \xi d\xi}, \quad (E1)$$

where ξ_n is defined as $p_n(\xi_n) = 1/2$ with n the order of the absorption process.

¹D. W. Pohl, W. Denk, and M. Lanz, *Appl. Phys. Lett.* **44**, 651 (1984).
²E. Betzig, A. Lewis, A. Harootunian, M. Isaacson, and E. Kratschmer, *Biophys. J.* **49**, 269 (1986).
³D. Courjon, K. Sarayeddine, and M. Spajer, *Opt. Commun.* **71**, 23 (1989).
⁴Y. Inoué and S. Kawata, *Opt. Lett.* **19**, 159 (1994).
⁵H. A. Bethe, *Phys. Rev.* **66**, 163 (1944).
⁶U. C. Fischer and D. Pohl, *Phys. Rev. Lett.* **62**, 458 (1989).
⁷F. Zenhausern, M. Oboyle, and H. Wickramasinghe, *Appl. Phys. Lett.* **65**, 1623 (1994).
⁸F. Zenhausern, Y. Martin, and H. Wickramasinghe, *Science* **269**, 1083 (1995).
⁹J. Jersch, F. Demming, and K. Dickman, *Appl. Phys. A: Mater. Sci. Process.* **64**, 29 (1997).
¹⁰J. Jersch, F. Demming, L. Hildenhagen, and K. Dickmann, *Appl. Phys. A: Mater. Sci. Process.* **66**, 29 (1998).
¹¹I. Smolyaninov, M. Khaikin, and V. Edelman, *Phys. Lett. A* **149**, 410 (1990).
¹²D. Abraham, A. Veider, C. Schönenberger, H. Meier, D. Arent, and S. Alvarado, *Appl. Phys. Lett.* **56**, 1564 (1990).
¹³R. Berndt, R. Gaisch, J. Gimzewski, B. Reihl, R. Schlittler, W. Schneider, and M. Tschudy, *Science* **262**, 1425 (1993).
¹⁴R. Berndt, R. Gaisch, W. Schneider, J. Gimzewski, B. Reihl, R. Schlittler, and M. Tschudy, *Appl. Phys. A: Solids Surf.* **57**, 513 (1993).
¹⁵R. Berndt, *Scanning Microsc.* **9**, 687 (1995).
¹⁶R. Berndt and J. Gimzewski, *Annalen Der Physik* **2**, 133 (1993).
¹⁷P. Liao and A. Wokaun, *J. Chem. Phys.* **76**, 751 (1982).
¹⁸P. J. Feibelman, *Prog. Surf. Sci.* **12**, 287 (1982).
¹⁹W. Denk and D. W. Pohl, *J. Vac. Sci. Technol. B* **9**, 510 (1991).
²⁰L. Novotny, E. Sanchez, and X. Xie, *Ultramicroscopy* **71**, 21 (1998).
²¹E. Betzig, J. K. Trautman, T. D. Harris, J. S. Weiner, and R. L. Kostelak, *Science* **251**, 1468 (1991).
²²O. Bouevitch, A. Lewis, and L. Loew, *Biophys. J.* **70**, 431A (1996).
²³A. Wokaun, *Mol. Phys.* **56**, 1 (1985).
²⁴W. Denk, J. H. Strickler, and W. W. Webb, *Biophys. J.* **57**, 374A (1990).
²⁵W. Denk, D. W. Piston, and W. W. Webb, in *The Handbook of Confocal Microscopy*, 2nd ed., edited by J. Pawley (Plenum, New York, 1995), p. 445–458.
²⁶W. Denk, *J. Biomed. Opt.* **1**, 296 (1996).
²⁷S. Soper, H. Nutter, R. Keller, L. Davis, and E. Shera, *Photochem. Photobiol.* **57**, 972 (1995).
²⁸C. Xu, W. Zipfel, J. Shear, R. Williams, and W. Webb, *Proc. Natl. Acad. Sci. USA* **93**, 10763 (1996).
²⁹B. Collings, J. Stark, S. Tsuda, W. Knox, J. Cunningham, W. Jan, R. Pathak, and K. Bergman, *Opt. Lett.* **21**, 1171 (1996).
³⁰T. Tsun, M. Islam, and P. Chu, *Opt. Commun.* **141**, 65 (1997).
³¹P. W. Barber, R. K. Chang, and H. Massoudi, *Phys. Rev. B* **27**, 7251 (1983).
³²H. S. Carslaw and J. C. Jaeger, *Conduction of Heat in Solids*, 2nd ed. (Oxford University Press, London, 1959).
³³W. Lukosz and R. Kunz, *J. Opt. Soc. Am.* **67**, 1615 (1977).
³⁴R. Chance, A. Prock, and R. Sibley, *Adv. Chem. Phys.* **60**, 1 (1978).
³⁵R. Chance, A. Prock, and R. Sibley, *J. Chem. Phys.* **60**, 2744 (1974).
³⁶R. Chance, A. Prock, and R. Sibley, *J. Chem. Phys.* **65**, 2527 (1974).
³⁷B. Stuart, M. Feit, S. Herman, A. Rubenchik, B. Shore, and M. Perry, *Phys. Rev. B* **53**, 1749 (1996).
³⁸R. Rigler, *J. Biotechnology* **41**, 177 (1995).
³⁹J. D. Harding and R. A. Keller, *Trends Biotechnol* **10**, 55 (1992).
⁴⁰W. Denk, *Proc. Natl. Acad. Sci. USA* **91**, 6629 (1994).
⁴¹E. Betzig, J. Trautman, R. Wolfe, E. Gyorgy, and P. Finn, *Appl. Phys. Lett.* **61**, 142 (1992).
⁴²A. Moussiaux, A. Ronveaux, and A. Lucas, *Can. J. Phys.* **55**, 1423 (1977).